Spin susceptibility in three-dimensional nearly magnetic disordered fermion systems in the weakly localized regime

M. T. Béal-Monod

Laboratoire de Physique des Solides, Université de Paris—Sud, F-91400 Orsay, France

(Received 15 April 1985)

The temperature dependence of the spin susceptibility $\chi(T)$ is studied in a weakly disordered itinerant-fermion system close to a magnetic instability. The paramagnon model is used with a Hubbard-type contact repulsion among opposite spins, with the Stoner enhancement of the pure system $(1-\bar{I})^{-1} \gg 1$. The result is shown to be different from the usual one obtained in the case of a screened Coulomb interaction: The 2-phDP (two—particle-hole-diffusion-propagator) diagrams, which cancel altogether in the Coulomb interaction case, are shown to give, here, for the contact interaction, a finite contribution which is of the same order in $(\varepsilon_F \tau)^{-1}$ as the 3-phDP and 4-phDP diagrams where τ is the lifetime due to disorder, and ε_F the Fermi energy. Instead of a unique temperature range $T\tau \ll 1$ in the Coulomb case, here one has to distinguish two ranges: When $T\tau \ll (1-\bar{I})$, the usual 3- and 4-phDP diagrams dominate and one recovers $\chi(T) \approx \sqrt{T\tau}/(1-\bar{I})^2$ as was first announced by Al'tshuler and Aronov; but when $(1-\bar{I}) < T\tau \ll 1$, the 2-phDP diagrams dominate, yielding $\chi(T) \sim (T\tau)^{3/2}/(1-\bar{I})^{5/2}$, which is non-negligible near the magnetic instability. At $T=0$, the 2-phDP diagrams definitely dominate as they enhance the effective interaction $(\bar{I}_{\text{eff}} - \bar{I}) \approx (\varepsilon_F \tau)^{-2}(1-\bar{I})^{-1/2}$ and let the system be closer to magnetism, while the 3- and 4-phDP diagrams play a minor role at 0 K. The present study accounts only for phDP processes. Effects due to ppDP's (particle-particle diffusion propagators) should also be studied within the same framework to incorporate the contributions of the 2-ppDP diagrams. Finally, the latest developments using renormalization-group analysis of Finkel'stein and of Castellani *et al.* with a screened Coulomb interaction ought to be modified to account for the contact-interaction case where spin constraints yield the noncancellation of the 2-phDP—and also most likely of the 2-ppDP—diagrams.

I. INTRODUCTION

The purpose of the present paper is to examine how the low-temperature dependence of the spin susceptibility $\chi(T)$ in a disordered fermion system is modified in the weakly localized regime ($\tau^{-1} \ll \epsilon_F$, τ being the lifetime due to the elastic impurity scattering, ϵ_F the Fermi energy), when the system is close to a magnetic instability $(1-\bar{I}) \simeq 0$, $\bar{I}$ being the dimensionless, Hubbard-type contact and instantaneous repulsion among opposite spins, $\bar{I} = I N_0$, where N_0 is the density of states at the Fermi energy for one spin direction, $N_0 = P_F/(2\pi^2)$ in atomic units. A short comment concerning this problem was given in Ref. 1, indicating a quantum modification to χ, in the weakly localized regime, $\delta\chi \sim T^{1/2}(1-\bar{I})^{-2}$, but the derivation of the $\bar{I}$ dependence is not given and the corresponding modification at $T=0$ was not provided. On the other hand in Ref. 2 inclusion of higher-order interaction effects in the weakly localized regime (the Hubbard type of interaction) was considered, and the following formula was obtained:

$$\delta\chi_{\text{IF}} = \chi_{\text{Pauli}}(1-\bar{I})^{-2}(\epsilon_F\tau)^{-2}[1-(1-\bar{I})^{1/2}]$$

$$\times (3\sqrt{3}/4)[1-0.73(2\pi T\tau)^{1/2}] \ . \qquad (1)$$

[The above formula is obtained from formulas (6.1) and (6.3) of Ref. 2 in the case where the T matrix is not used, i.e., with $F/2$ replaced by $\bar{I}/(1-\bar{I})$ in the present nota-

tion.] In (1), the $T=0$ as well as the finite-T contribution to $\delta\chi$ is provided.

I wish to reexamine the derivation of $\delta\chi$. The motivation is that, according to the calculation of $\chi(T)$ in the pure case[3] for the paramagnon contribution to $\chi(T)$ some diagrams do not seem to have been considered in Refs. 1 and 2 and some other were assumed to cancel, as they indeed do in the Coulomb-interaction case, while they do not for the present contact interaction case. Although the $(1-\bar{I})^{-2}(T\gamma)^{1/2}$ contribution of Refs. 1 and 2 is present in both cases, the $\bar{I}$ dependence in the numerator of (1) is slightly modified here, but it still does not diverge when $\bar{I} \to 1$; however, what is more important is that the contribution due to diagrams which were supposed to cancel in Ref. 2 and 1 introduces here terms proportional to $(1-\bar{I})^{-5/2}(T\tau)^{3/2}$; such a contribution may be either negligible compared to the above $(1-I)^{-2}(T\tau)^{1/2}$, or important depending on the range of T, [i.e., depending on $T\tau$ as compared to $(1-\bar{I})^{1/2}$, both quantities being much smaller than unity]. In any case, at $T=0$, the contribution due to the diagrams which were supposed to cancel in Ref. 2 predominates here as it contains an extra factor $(1-\bar{I})^{-1/2}$. This last point is very important in connection with computation of the "effective" value of $\bar{I}$, (the $\bar{I}_{\text{eff}}$ considered in Ref. 4), renormalized by disordered paramagnons of use to quantitatively check whether the effective susceptibility enhancement $(1-\bar{I}_{\text{eff}})^{-1}$ is larger or smaller than the bar one $(1-\bar{I})^{-1}$. This point is also
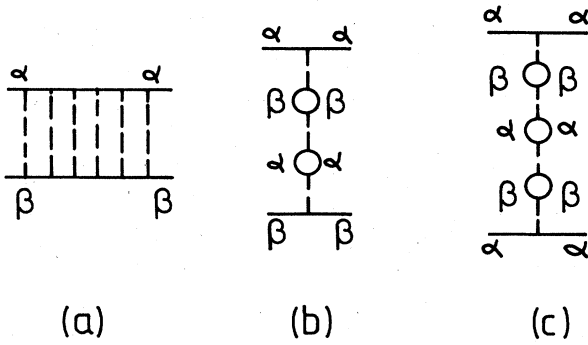
       ©1985 The American Physical Society

(a)   (b)   (c)

FIG. 1. Three kinds of possible paramagnon structures, in the absence of disorder (which will be schematized as a wiggly line in Fig. 3); α and β refer to the spin orientations of the fermion lines (the solid ones), $\alpha = -\beta = \pm 1$. Dashed line is the bare contact repulsion I among opposite spins: (a) transverse paramagnon containing an infinite ladder in the interaction; (b) and (c) are longitudinal paramagnons containing an infinite, respectively even and odd, number of elementary bubbles.

important in connection with the most recent developments[5] on disordered electron systems where screened Coulomb interactions were considered. These studies, in principle, cover the short-range as well as the long-range interaction case. However, it is shown here that the problem appears to be slightly more subtle. The short-range case forces one to consider not just one diagrammatic structure for the interaction propagator (as for the case of a screened Coulomb interaction), but three different ones for the three different paramagnon propagators (this is made explicit in Fig. 1 in the absence of disorder). This very point is responsible for the noncancellation of the diagrams containing 2- as well as 3-phDP (particle-hole-diffusion-propagator) processes, and for the combination among some other diagrams containing 4-phDP processes which give a contribution of the same order in $(\epsilon_F \tau)$ as the 3-phDP processes.

II. BRIEF REVIEW OF THE LOWEST-ORDER PARAMAGNON CONTRIBUTION TO THE SUSCEPTIBILITY IN THE PURE CASE

For pedagogical reasons it is useful to start with a brief review of the lowest-order paramagnon contribution to χ in the absence of disorder[3] and, first of all, of some well-known basic ingredients entering in the calculation of χ. This will prove extremely useful for an understanding of the disordered case.

To compute the static susceptibility, one needs to evaluate the spin-spin correlation function $\langle S^z S^z \rangle$, i.e., the longitudinal susceptibility χ^{zz}:

$$\chi^{zz} = \langle S^z S^z \rangle = \left[\frac{n_+ - n_-}{2} \right] \left[\frac{n_+ - n_-}{2} \right] , \qquad (2)$$

where $n_\pm$ are the spin-up or -down densities. Since, by symmetry $n_+ n_+ = n_- n_-$ and $n_- n_+ = n_+ n_-$, one is left with
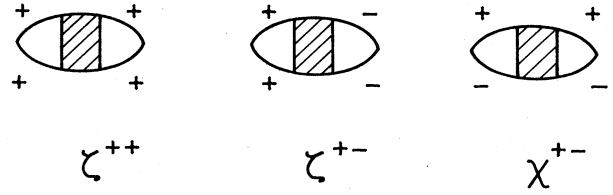

FIG. 2. Diagrams entering into the calculation of χ^{zz} [ζ^{++} and ζ^{+-} of formula (3)], and of χ^{+-} of formula (4). The signs of the fermion lines (the solid lines) are the spin directions. Shaded area is made explicit in Fig. 3.

$$\chi^{zz} = \langle S^z S^z \rangle = \frac{\zeta^{++} - \zeta^{+-}}{2} ,$$

where

$$\zeta^{++} = n_+ n_+ \quad \text{and} \quad \zeta^{+-} = n_+ n_- . \qquad (3)$$

On the other hand, the transverse susceptibility χ^{+-} is given by

$$\chi^{+-} = \chi^{xx} + \chi^{yy} . \qquad (4)$$

When the magnetic field is turned off, one gets, as is well known,

$$\chi^{xx} = \chi^{yy} = \chi^{zz} = \tfrac{1}{2}\chi^{+-} \quad (\text{for } H = 0) , \qquad (5)$$

in which case (the field $H \to 0$)

$$\chi^{+-} = \zeta^{++} - \zeta^{+-} \quad (\text{for } H = 0) . \qquad (6)$$

The diagrams corresponding to the three quantities ζ^{++}, ζ^{+-}, and χ^{+-} are schematically given on Fig. 2. To lowest order in a paramagnon insertion, any block (shaded area of Fig. 2) contains the various possibilities indicated on Fig. 3. On the other hand, the paramagnon (wiggly line on Fig. 3), may have the three kinds of structures exhibited in Fig. 1; since the interaction I arises only among opposite spins, one may have either a transverse paramagnon, Fig. 1(a), with an infinite ladder in the interaction I, or two longitudinal paramagnons, Fig. 1(b), containing an even number of elementary bubbles $(2l)$, with $l \to \infty$, when the spins of the two external fermion lines are opposite, or Fig. 1(c), with an odd number of bubbles $(2l + 1)$, with $l \to \infty$, when the spins of the two external lines are the same. While the effective interactions between the external fermion lines with opposite spins [Figs. 1(a) and 1(b)] are repulsive, like the bare one I, in contrast, the effective paramagnon-mediated interaction entering into Fig. 1(c) has *one elementary bubble difference* compared with Fig. 1(b), and therefore one minus sign difference (so that the resulting effective interaction is attractive among parallel spins). This remark
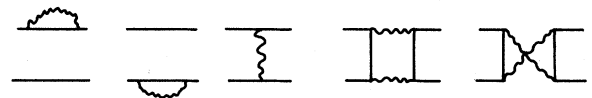

FIG. 3. The lowest-order paramagnon contribution entering in the shaded area of Fig. 2. Wiggly lines are paramagnons of the various kinds in Fig. 1. Solid lines are fermion lines.
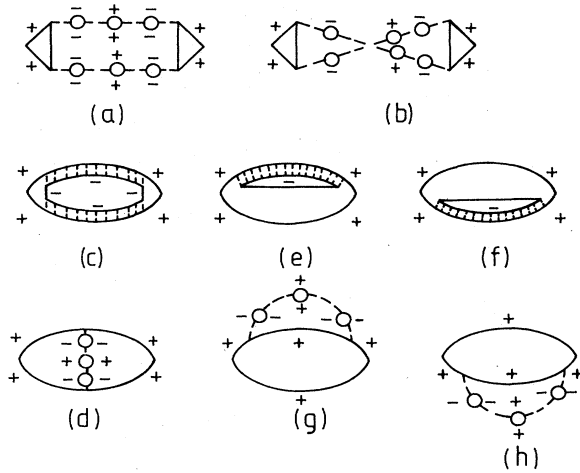
FIG. 4. Diagrams contributing to the ζ^{++} part of the longitudinal susceptibility in formula (3) (each bubble string contains an odd number of such bubbles).

will be the key point in the following; the same remark has allowed one in the past to propose[6] that paramagnons favor triplet-pairing superconductivity, although they suppress singlet-pairing superconductivity. One can now draw the various diagrams contributing (to lowest order in the paramagnon insertion), to either the longitudinal susceptibility through ζ^{++} and ζ^{+-} (Figs. 4 and 5), or to the transverse one χ^{+-} (Fig. 6.) It is easy to check mathematically that, as $H \rightarrow 0$, the sum of the diagrams involved in $(\zeta^{++} - \zeta^{+-})$ is equal to the one involved in χ^{+-}. Therefore, depending whether one or the other way is more convenient, it is equivalent to compute the static susceptibility by deriving the free energy twice with respect to the magnetic field H (i.e., to cut two fermion lines in the diagrams of Fig. 7), which yield the longitudinal susceptibility through $(\zeta^{++} - \zeta^{+-})$ or to compute χ^{+-} by calculating the four types of diagrams of Fig. 8, whose details are given in Fig. 6. It was shown in Ref.
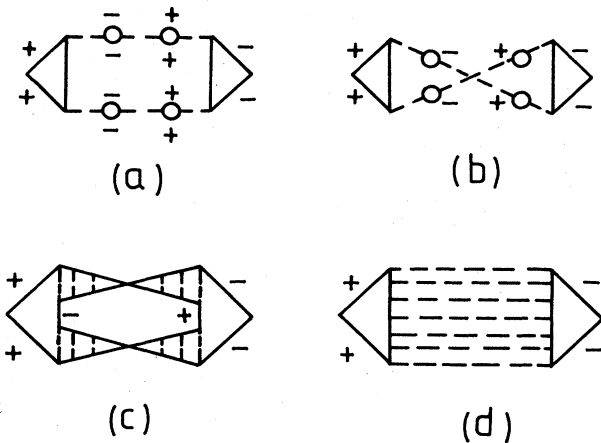

FIG. 5. Diagrams contributing to the ζ^{+-} part of the longitudinal susceptibility in formula (3) (each bubble string contains an even number of such bubbles).
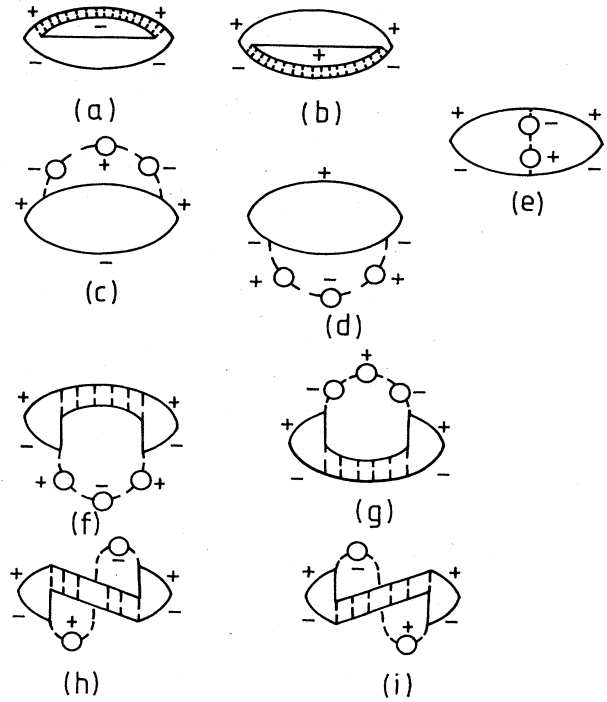

FIG. 6. Diagrams contributing to the transverse susceptibility χ^{+-} (c), (d), (f), and (g) contain an odd number of bubbles; (e), (h), and (i) contain an even number of bubbles.

3(b) as well as in the rotationally invariant formulation of Ref. 7 that the last two diagrams of Fig. 8 combine to yield a contribution of the same order in the divergent parameter $(1 - \bar{I})^{-1}$ as that of the first two. A different but analogous combination will appear in the following, of crucial importance in the disordered case.

To end this first part, I wish to clearly specify the notations used in this paper, as was used in the pure case of Ref. 3. A dashed line as in Figs. 1 and 4—7 represents the bare contact interaction with a minus sign, $-I$; a solid (fermion) line represents a fermion Green's function with a minus sign, $-G$; a closed loop will have a minus sign, so that each bare bubble in the preceding diagrams is
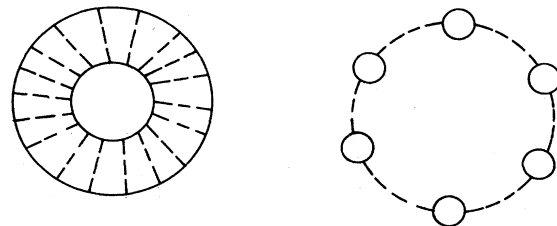

FIG. 7. Free-energy diagrams generating the paramagnon contribution to the longitudinal susceptibility, constructed by cutting two fermion lines in all possible ways, as was done in the pure case of Ref. 3. (Note that the second diagram contains an even or odd number of bubbles in the presence of a field; it is only when the field is turned off that one must have spin conservation, yielding the only possibility shown in Figs. 4, 5, and 6.)
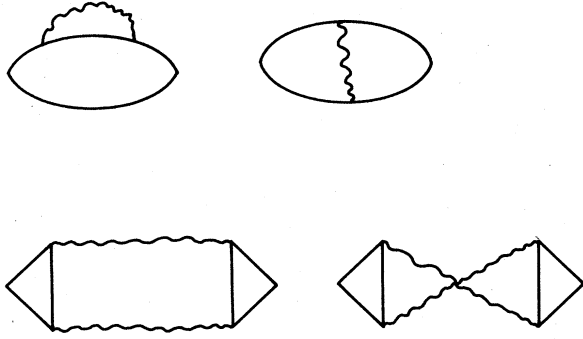
FIG. 8. Diagrams of Fig. 6 schematized in order to make a link with the disordered ones involved in the remainder of the paper.

FIG. 9. The phDP-type diagrams Λ (top line) and Γ (bottom line) exhibiting infinite scatterings of the fermions on the impurities (the crosses are impurities and the dotted lines correspond to the scattering potential). Here each fermion line (solid lines) is also renormalized by impurity scatterings.

$\chi_0 = (-1) \sum (-G)(-G) = -\sum GG$, where the sum is over momentum and frequency variables. The same notation will be used later on in this paper when fermion lines will be renormalized by impurity scattering and the "disordered" elementary bubble $\widetilde{\chi}_0$ will include vertex corrections due to impurity scattering and fermion lines also renormalized by impurity scattering [as will be explicated later in connection with Fig. 11(a) and Λ in Fig. 9].

III. THE LOWEST-ORDER PARAMAGNON CONTRIBUTIONS TO THE SPIN SUSCEPTIBILITY IN THE DISORDERED CASE WITH 2-, 3- , AND 4- phDP PROCESSES

A. Noncancellation of 2-phDP diagrams

I now turn to the case where a mean free path due to a weak disorder dresses the preceding quantities. It appears easier to compute the static susceptibility through χ^{+-} which contains less diagrams than χ^{zz} since, in the limit of zero field, both ways are equivalent. As in Refs. 1 and 2, I restrict myself to the "weak-localization" regime:

$$\epsilon_F \tau \gg 1 \ . \tag{7}$$

The diagrams of Fig. 6 will now be dressed with impurity scattering; a fermion Green's function now reads

$$G(\mathbf{p}, \widetilde{\omega}_n) = (i\widetilde{\omega}_n - \xi_{\mathbf{p}})^{-1} \tag{8}$$

with the standard notation[8] for Matsubara frequencies,

$$\widetilde{\omega}_n = \omega_n + \frac{1}{2\tau} \mathrm{sgn}\omega_n \ ,$$

$$\omega_n = 2\pi T(n + \tfrac{1}{2}), \quad n = 0, 1, 2, \cdots \tag{9}$$

and (in atomic units) with

$$\xi_{\mathbf{p}} = \frac{p^2}{2} - \frac{p_F^2}{2} \ . \tag{10}$$

On the other hand, for simplicity, I restrict my considerations to the vertex corrections due to impurity scattering to be only of the "diffuson" type, or particle-hole diffusion propagators (phDP's) containing an infinite ladder of impurity scattering as usual,[1,2,9] and recalled in Fig. 9:
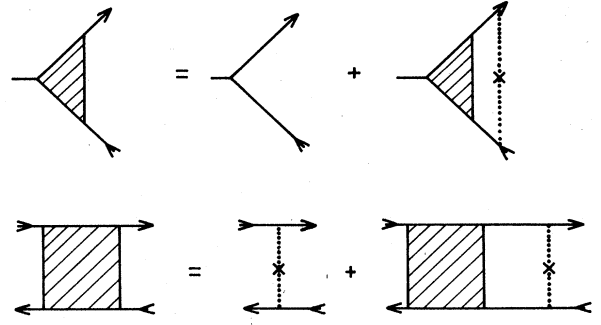
$$\Lambda(q, |\omega_v|) = \tau^{-1}(Dq^2 + |\omega_v|)^{-1} \ ,$$

$$D = p_F^2 \tau/3 \ ,$$

$$\Gamma(q, |\omega_v|) = (2\pi N_0 \tau^2)^{-1}(Dq^2 + |\omega_v|)^{-1} \tag{11}$$

$$= \Lambda/(2\pi N_0 \tau) \ ,$$

$$\omega_v = 2\pi v T, \quad v = 0, 1, 2, \cdots$$

where Λ and Γ are computed in the diffusive regime, and one has the usual conditions[1,2,9]

$$k_F q \tau \ll 1 \ ,$$

$$|\omega_v|\tau \ll 1 \ , \tag{12}$$

$$T\tau \ll 1 \ .$$

With the help of Λ and Γ, one can compute the basic diagrams of Fig. 10 which serve to compute the various disordered paramagnon propagators. The disordered bubble $\widetilde{\chi}_0(q, |\omega_v|)$ [the closed loop of Fig. 10(a)] is [with the conventions of Sec. II and with Eqs. (8)–(11)]

$$\widetilde{\chi}_0(q, |\omega_v|) = -T \sum_n \int \frac{d^3\mathbf{p}}{(2\pi)^3} G(\mathbf{p}, \widetilde{\omega}_n)$$

$$\times G(\mathbf{p}+\mathbf{q}, \widetilde{\omega}_{n+v}) \Lambda(q, |\omega_v|)$$

$$= N_0 - T \sum_{n=0}^{v-1} 2\pi\tau N_0 \Lambda \left[\frac{\Lambda-1}{\Lambda} \right]$$

$$= N_0 \frac{Dq^2}{Dq^2 + |\omega_v|} \ . \tag{13}$$

[Note that as Λ is divergent for small q and $|\omega_v|$, $(\Lambda-1) \sim \Lambda$.] The quantity displayed in Fig. 10(b), $\widetilde{\chi}_0$, is
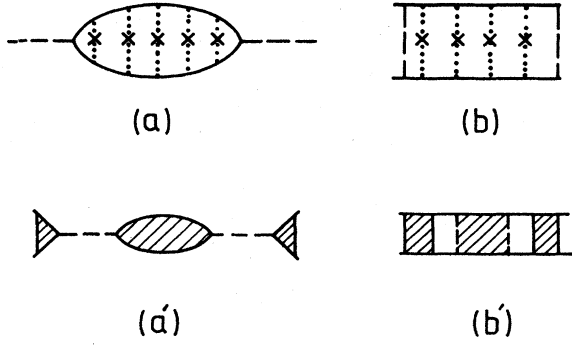
FIG. 10. The basic ingredients $\widetilde{\chi}_0$ [in (a)] and $\overline{\chi}_0$ [in (b)] of (13) and (14) and the corresponding lowest-order (in the interaction) contribution to the disordered paramagnons $\widetilde{\chi}_{ro}$ or $\widetilde{\chi}_{re}$ [in (a')] and $\widetilde{\chi}_l$ [in (b')]. All fermion lines (solid lines) are themselves renormalized by impurity scattering. Notation is the same as in Fig. 9.

$$\overline{\chi}_0(q,|\omega_\nu|) = T \sum_n \int \frac{d^3\mathbf{p}}{(2\pi)^3} G(\mathbf{p},\widetilde{\omega}_n)G(\mathbf{p}+\mathbf{q},\widetilde{\omega}_{n+\nu})$$

$$\times \Gamma(q,|\omega_\nu|) \int \frac{d^3\mathbf{p}'}{(2\pi)^3} G(\mathbf{p}',\widetilde{\omega}_n)$$

$$\times G(\mathbf{p}'+q,\widetilde{\omega}_{n+\nu})$$

$$= - \left[N_0 - T \sum_{n=0}^{\nu-1} (2\pi N_0\tau)^2 \Gamma \left[\frac{\Lambda-1}{\Lambda}\right]^2 \right]$$

$$= -N_0 \frac{Dq^2}{Dq^2+|\omega_\nu|} = -\widetilde{\chi}_0 . \tag{14}$$

Then if one computes the disordered paramagnons (corresponding to those of Fig. 1, but in the presence of disorder), one gets for their lowest-order contribution displayed in Figs. 10(a') and 10(b'), with the use of (11),

Diagram $[10(a')] \rightarrow (-I)^2\Lambda^2\widetilde{\chi}_0 = I^2\Lambda^2\widetilde{\chi}_0$ (15a)

Diagram $[10(b')] \rightarrow (-I)^2\Gamma^2\widetilde{\chi}_0 \left[N_0 2\pi\tau\frac{\Lambda-1}{\Lambda}\right]^2$

$$= (-I)^2 \left[(2\pi N_0\tau\Gamma)\frac{\Lambda-1}{\Lambda}\right]^2 \widetilde{\chi}_0$$
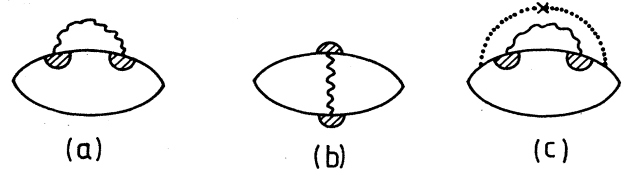
$$= I^2\Lambda^2(-\widetilde{\chi}_0) . \tag{15b}$$

FIG. 11. The same conductivity diagrams as in Figs. 5(a), 5(b), and 5(c) of Ref. 10 containing 2 phDP's. They cancel when the wiggly line is the screened Coulomb interaction, but they do not cancel when it is a disordered paramagnon (see details in Appendix A), in which case they contribute a term of $(T\tau)^{3/2}$ to the conductivity as well as to the susceptibility. As in Ref. 10, there are two diagrams like (a), and two diagrams like (c), when the self-energy affects the "hole" line instead of the electron line.

This will serve as the basic ingredients in what I will call $\widetilde{\chi}_{ro}$, $\widetilde{\chi}_{re}$, and $\widetilde{\chi}_l$ as being disordered paramagnons containing, respectively, an odd and an even number of disordered closed bubbles and an infinite interaction ladder.

I first examine here the diagrams of Fig. 11 containing 2 phDP's renormalizing the vertices at the meeting points between the wiggly line and the fermion line. Such diagrams were shown to cancel in the Coulomb interaction case.[1,2,9] The cancellation has been shown explicitly in great detail in Appendix C of Ref. 10 where the conductivity diagrams of Fig. 11 were computed in two dimensions, with the wiggly line being the screened Coulomb interaction $V_s(q,\omega)$. I compute, in Appendix A of the present paper, the same conductivity diagrams in three dimensions, but the dimensionality plays no role in the cancellation or noncancellation of these diagrams. I keep track of the various contributions until the very end, where I find the following: (i) when the wiggly line in Fig. 11 is the screened Coulomb interaction $V_s(q,\omega)$ of Ref. 10, I recover the result of that reference that the diagrams altogether cancel; in contrast, (ii) when the wiggly line is the appropriate disordered paramagnon [$\widetilde{\chi}_{ro}$ and $\widetilde{\chi}_l$ in Figs. 11 (a) and 11(c) and $\widetilde{\chi}_{re}$ in Fig. 11(b)], the diagrams do not cancel, but combine to yield a nonvanishing contribution (independently of the dimensionality being two or three).

The absence of cancellation in (ii) is only due to the geometrical structure of the involved paramagnons containing an even or odd number of elementary bubbles depending on the spin directions of the fermions lines at both ends.

In what follows, I compute directly the corresponding susceptibility diagrams in three dimensions. As for the conductivity, and for the same reason, the susceptibility diagrams containing 2 phDP's do not cancel. The sum of the diagrams with a self-energy correction containing a disordered paramagnon with an odd number of bubbles $\widetilde{\chi}_{ro}$ and the diagram with a vertex correction containing a disordered paramagnon with an even number of bubbles $\widetilde{\chi}_{re}$ read

$$
(\delta\chi_{ro}+\delta\chi_{re})_{2\ \text{phDP}} = \left[-2T^2 \sum_{n,\nu} \int \frac{d^3\mathbf{p}}{(2\pi)^3} \int \frac{d^3\mathbf{q}}{(2\pi)^3} G^3(\mathbf{p},\widetilde{\omega}_n)G(\mathbf{p}+\mathbf{q},\widetilde{\omega}_{n+\nu})\Lambda^2(q,|\omega_\nu|)\frac{I^2\widetilde{\chi}_0}{1-I^2\widetilde{\chi}_0^2} \right]
$$

$$
+ \left[-T^2 \sum_{n,\nu} \int \frac{d^3\mathbf{p}}{(2\pi)^3} \int \frac{d^3\mathbf{q}}{(2\pi)^3} G^2(\mathbf{p},\widetilde{\omega}_n)G^2(\mathbf{p}+\mathbf{q},\widetilde{\omega}_{n+\nu})\Lambda^2(q,|\omega_\nu|) \right] \left[-\frac{I^3\widetilde{\chi}_0^2}{1-I^2\widetilde{\chi}_0^2} \right]
$$

$$
= 2T \sum_\nu |\omega_\nu| \int \frac{d^3\mathbf{q}}{(2\pi)^3} \Lambda^2 N_0 \tau^3 \left[\left[\frac{I^2\widetilde{\chi}_0}{1-I^2\widetilde{\chi}_0^2} \right] - \left[-\frac{I^3\widetilde{\chi}_0^2}{1-I^2\chi_0^2} \right] \right] . \tag{16}
$$

In (16) and in the following, I use the results displayed in Appendix B for a number of integrals, over momentum, of various products of fermion Green's functions. If, in the right-hand side of (16), one would have inside both parentheses the same Coulomb propagator $V_s(q,|\omega_\nu|)$, the difference of them would vanish as it does in Ref. 1, 2, 9, and 10. Instead, here, again because of the different structures of the involved paramagnons, the same quantity does not vanish:

$$
(\delta\chi_{ro}+\delta\chi_{re})_{2\ \text{phDP}} = 2N_0\tau^3 T \sum_\nu |\omega_\nu| \int \frac{d^3\mathbf{q}}{(2\pi)^3} \Lambda^2 \frac{I^2\widetilde{\chi}_0}{1-I\widetilde{\chi}_0} . \tag{17}
$$

The various paramagnon propagators used above, and in the following, read as follows:

$$
\widetilde{\chi}_{ro}(q,|\omega_\nu|) = +\frac{I^2\widetilde{\chi}_0(q,|\omega_\nu|)}{1-I^2\widetilde{\chi}_0^2(q,|\omega_\nu|)} , \tag{18a}
$$

$$
\widetilde{\chi}_{re}(q,|\omega_\nu|) = -\frac{I^3\widetilde{\chi}_0^2(q,|\omega_\nu|)}{1-I^2\widetilde{\chi}_0^2(q,|\omega_\nu|)} , \tag{18b}
$$

$$
\widetilde{\chi}_I(q,|\omega_\nu|) = -\frac{I^2\widetilde{\chi}_0(q,|\omega_\nu|)}{1-I\widetilde{\chi}_0(q,|\omega_\nu|)} . \tag{18c}
$$

The lowest order (in the interaction) of (18a) and (18c) multiplied by the vertex correction Λ^2 was computed in (15); note the sign difference between (18a) and (18b) corresponding to one bubble difference between them. Recall that, in computing (16) and in order to get the diffusion pole in Λ as given in (11) (the most singular term), one must have for the fermion Green's-function frequencies

$$
(\omega_n,\omega_{n+\nu}) < 0 . \tag{19}
$$

Now, to the contribution (17), one must also add the diagrams with a self-energy correction containing a disordered paramagnon of ladder type in the interaction $\widetilde{\chi}_I$ as given by (18c):

$$
(\delta\chi_I)_{2\ \text{phDP}} = 2T^2 \sum_{n,\nu} \int \frac{d^3\mathbf{p}}{(2\pi)^3} \int \frac{d^3\mathbf{q}}{(2\pi)^3} G^3(\mathbf{p},\widetilde{\omega}_n)G(\mathbf{p}+\mathbf{q},\widetilde{\omega}_{n+\nu})\Lambda^2 \left[-\frac{I^2\widetilde{\chi}_0}{1-I\widetilde{\chi}_0} \right]
$$

$$
= 2N_0\tau^3 T \sum_\nu |\omega_\nu| \int \frac{d^3\mathbf{q}}{(2\pi)^3} \Lambda^2 \frac{I^2\widetilde{\chi}_0}{1-I\widetilde{\chi}_0} . \tag{20}
$$

Therefore this last contribution is equal to the one given above in (17). Then the sum of the contributions with 2 phDP's is

$$
(\delta\chi_{ro}+\delta\chi_{re}+\delta\chi_I)_{2\ \text{phDP's}} = 4N_0\tau^3 T \sum_\nu |\omega_\nu| \int \frac{d^3\mathbf{q}}{(2\pi)^3} \Lambda^2 \frac{I^2\widetilde{\chi}_0}{1-I\widetilde{\chi}_0}
$$

$$
= 4\bar{I}^2 \tau T \sum_\nu |\omega_\nu| \int \frac{d^3\mathbf{q}}{(2\pi)^3} \frac{Dq^2}{(Dq^2+|\omega_\nu|)^2[(1-\bar{I})Dq^2+|\omega_\nu|]}
$$

$$
= \frac{\tau}{\pi} \frac{1}{D^{3/2}} \left[\frac{1}{(1-\bar{I})^{1/2}} - 1 - \frac{\bar{I}}{2} \right] T \sum_\nu \sqrt{|\omega_\nu|}
$$

$$
= \frac{\sqrt{3}N_0}{(\epsilon_F\tau)^2} \left[\frac{1}{(1-\bar{I})^{1/2}} - 1 - \frac{\bar{I}}{2} \right] [1-(2\pi T\tau)^{3/2}] . \tag{21}
$$

One can check that $[(1-\overline{I})^{-1/2}-1-\overline{I}/2]$ vanishes, as it should, when $\overline{I}\to 0$ like $\overline{I}^{2}$, and, on the other hand, diverges like $(I-\overline{I})^{-1/2}$ when the magnetic instability is approached, $\overline{I}\to 1$. Note that the sum over ω_{ν} is restricted to $|\omega_{\nu}|\tau<1$.

B. Diagrams with 3- and 4-phDP processes

1. 3 phDP's

I concentrate first on 3-phDP processes [Fig. 4 of Ref. 9 or Fig. 5(a)—5(d) of Ref. 2, or here, Figs. 12(a), 12(a'), 12(b), and 12(b')], which cancel among themselves if the wiggly line is the screened Coulomb interaction and which, in the present case, will combine since they involve $\widetilde{X}_{ro}$, $\widetilde{X}_{re}$, and $\widetilde{X}_{l}$. As I did with 2 phDP's, I first compute

$$(\delta X_{ro}+\delta X_{re})_{3\text{ phDP}}=\left[-2T^{2}\sum_{n,\nu}\int\frac{d^{3}\mathbf{p}}{(2\pi)^{3}}\int\frac{d^{3}\mathbf{p}'}{(2\pi)^{3}}\int\frac{d^{3}\mathbf{q}}{(2\pi)^{3}}G^{2}(\mathbf{p},\widetilde{\omega}_{n})G(\mathbf{p}+\mathbf{q},\widetilde{\omega}_{n+\nu})G^{2}(\mathbf{p}',\widetilde{\omega}_{n})\right.$$

$$\times G(\mathbf{p}'+\mathbf{q},\widetilde{\omega}_{n+\nu})\Gamma(q,|\omega_{\nu}|)\Lambda^{2}(q,|\omega_{\nu}|)\left.\left[\frac{I^{2}\widetilde{X}_{0}}{1-I^{2}\widetilde{X}_{0}^{2}}\right]\right]$$

$$+\left[-2T^{2}\sum_{n,\nu}\int\frac{d^{3}\mathbf{p}}{(2\pi)^{3}}\int\frac{d^{3}\mathbf{p}'}{(2\pi)^{3}}\int\frac{d^{3}\mathbf{q}}{(2\pi)^{3}}G^{2}(\mathbf{p},\widetilde{\omega}_{n})G(\mathbf{p}+\mathbf{q},\widetilde{\omega}_{n+\nu})G^{2}(\mathbf{p}'+\mathbf{q},\widetilde{\omega}_{n+\nu})\right.$$

$$\times G(\mathbf{p}',\widetilde{\omega}_{n})\Gamma(q,|\omega_{\nu}|)\Lambda^{2}(q,|\omega_{\nu}|)\left.\left[-\frac{I^{3}\widetilde{X}_{0}^{2}}{1-I^{2}\widetilde{X}_{0}^{2}}\right]\right]$$

$$=2T\sum_{\nu}|\omega_{\nu}|\int\frac{d^{3}\mathbf{q}}{(2\pi)^{3}}2\pi N_{0}\tau^{4}\Lambda^{2}\Gamma\left[\left[\frac{I^{2}\widetilde{X}_{0}}{1-I^{2}\widetilde{X}_{0}^{2}}\right]-\left[-\frac{I^{3}\widetilde{X}_{0}^{2}}{1-I^{2}\widetilde{X}_{0}^{2}}\right]\right].\tag{22}$$

To compute (22), I also use the integrals over Green's functions whose details are given in appendix B. Here, as in (15), if one would have $V_{s}(q,|\omega_{\nu}|)$ in each pair of parentheses of the last line, (22) would vanish as it does in Refs. 2 and 9. Instead I get

$$(\delta X_{ro}+\delta X_{re})_{3\text{ phDP}}=4\pi N_{0}^{2}\tau^{4}\sum_{\nu}|\omega_{\nu}|\int\frac{d^{3}\mathbf{q}}{(2\pi)^{3}}\Lambda^{2}\Gamma\frac{I^{2}\widetilde{X}_{0}}{1-I\widetilde{X}_{0}}.\tag{23}$$

On the other hand,

$$(\delta X_{l})_{3\text{ phDP}}=\left[2T^{2}\sum_{n,\nu}\int\frac{d^{3}\mathbf{p}}{(2\pi)^{3}}\int\frac{d^{3}\mathbf{p}'}{(2\pi)^{3}}\int\frac{d^{3}\mathbf{q}}{(2\pi)^{3}}G^{2}(\mathbf{p},\widetilde{\omega}_{n})G(\mathbf{p}+\mathbf{q},\widetilde{\omega}_{n+\nu})G^{2}(\mathbf{p}',\widetilde{\omega}_{n})G(\mathbf{p}'+\mathbf{q},\widetilde{\omega}_{n+\nu})\right.$$

$$\times \Gamma(q,|\omega_{\nu}|)\Lambda^{2}(q,|\omega_{\nu}|)\left.\left[-\frac{I^{2}\widetilde{X}_{0}}{1-I\widetilde{X}_{0}}\right]\right]$$

$$=4\pi N_{0}^{2}\tau^{4}\sum_{\nu}|\omega_{\nu}|\int\frac{d^{3}\mathbf{q}}{(2\pi)^{3}}\Lambda^{2}\Gamma\frac{I^{2}\widetilde{X}_{0}}{1-I\widetilde{X}_{0}},\tag{24}$$

and thus again this last contribution is equal to the one in (23). The sum of the contributions with 3-phDP processes is

$$(\delta X_{ro}+\delta X_{re}+\delta X_{l})_{3\text{ phDP}}=8\pi N_{0}^{2}\tau^{4}T\sum_{\nu}|\omega_{\nu}|\int\frac{d^{3}\mathbf{q}}{(2\pi)^{3}}\Lambda^{2}\Gamma\left[\frac{I^{2}\widetilde{X}_{0}}{1-I\widetilde{X}_{0}}\right].\tag{25}$$

Before proceeding with the detailed calculation of (25), I have also to consider diagrams with 4 phDP's.

2. 4 phDP's

I now compute the diagrams with 4 phDP's of the type of Figs. 12(c) and 12(d), which, in absence of disorder, correspond to those of Figs. 6(f)—6(i). They read

$$(\delta\chi)_{4\text{ phDP}}= \left[-2T^3 \sum_{n,n',\nu} \int \frac{d^3p}{(2\pi)^3} \int \frac{d^3p'}{(2\pi)^3} \int \frac{d^3q}{(2\pi)^3} G^2(\mathbf{p},\widetilde{\omega}_n)G(\mathbf{p+q},\widetilde{\omega}_{n+\nu})G^2(\mathbf{p}',\widetilde{\omega}_{n'})G(\mathbf{p'+q},\widetilde{\omega}_{n'+\nu}) \right.$$

$$\times \Lambda^4(q,|\omega_\nu|)\left[-\frac{I}{1-I\widetilde{\chi}_0}\right]\left[\frac{I^2\widetilde{\chi}_0}{1-I^2\widetilde{\chi}_0^2}\right]\Bigg]$$

$$+\left[-2T^3 \sum_{n,n',\nu} \int \frac{d^3p}{(2\pi)^3} \int \frac{d^3p'}{(2\pi)^3} \int \frac{d^3q}{(2\pi)^3} G^2(\mathbf{p},\widetilde{\omega}_n)G(\mathbf{p+q},\widetilde{\omega}_{n+\nu})G^2(\mathbf{p}',\widetilde{\omega}_{n'})G(\mathbf{p-q},\widetilde{\omega}_{n'-\nu}) \right.$$

$$\times \Lambda^4(q,|\omega_\nu|)\left[-\frac{I}{1-I\widetilde{\chi}_0}\right]\left[-\frac{I}{1-I^2\widetilde{\chi}_0^2}\right]\Bigg]$$

$$=2T\sum_\nu \omega_\nu^2 \int \frac{d^3q}{(2\pi)^3} N_0^2\tau^4\Lambda^4 \left[-\frac{I}{1-I\widetilde{\chi}_0}\right]\left\{\left[\frac{I^2\widetilde{\chi}_0}{1-I^2\widetilde{\chi}_0^2}\right]-\left[-\frac{I}{1-I^2\widetilde{\chi}_0^2}\right]\right\} . \tag{26}$$

Here too, if one had $V_s(q,|\omega_\nu|)$ in both sets of large parentheses in the last line, these diagrams would vanish as was found in Figs. 5(e) and 5(f) of Ref. 2, for instance. Instead, here, they combine to give

$$(\delta\chi)_{4\text{ phDP}}=2T\sum_\nu \omega_\nu^2 \int \frac{d^3q}{(2\pi)^3} N_0^2\tau^4\Lambda^4 \left[-\frac{I^2}{(1-I\widetilde{\chi}_0)^2}\right] . \tag{27}$$

Now, I combine the results obtained with 3- and 4-phDP processes, formulas (25) and (27), to get

$$(\delta\chi)_{3\text{ phDP}}+(\delta\chi)_{4\text{ phDP}}= \left[2\frac{\overline{I}^2}{\pi^2}T\sum_\nu |\omega_\nu| \int dq \frac{q^2}{(Dq^2+|\omega_\nu|)^3}\frac{Dq^2}{(1-\overline{I})Dq^2+|\omega_\nu|}\right]$$

$$+\left[-\frac{\overline{I}^2}{\pi^2}T\sum_\nu \omega_\nu^2 \int dq \frac{q^2}{(Dq^2+|\omega_\nu|)^2}\frac{1}{[(1-\overline{I})Dq^2+|\omega_\nu|]^2}\right] . \tag{28}$$

Straightforward algebraic manipulations yield

$$(\delta\chi)_{3\text{ phDP}}+(\delta\chi)_{4\text{ phDP}}= \frac{1}{4\pi D^{3/2}}\left[1-\frac{\overline{I}}{2}-(1-\overline{I})^{1/2}\right]T\sum_\nu \frac{1}{|\omega_\nu|^{1/2}}$$

$$=\frac{3\sqrt{3}}{4}\frac{N_0}{(\epsilon_F\tau)^2}\left[1-\frac{\overline{I}}{2}-(1-\overline{I})^{1/2}\right][1-(2\pi T\tau)^{1/2}] . \tag{29}$$
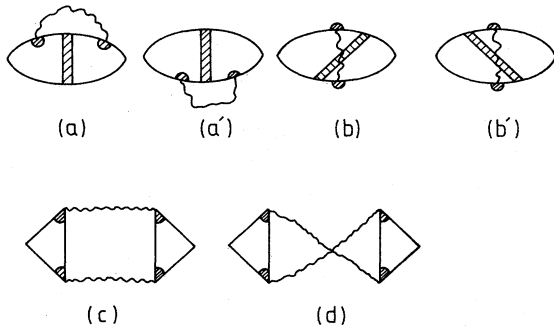

(a) (a') (b) (b')

(c) (d)

FIG. 12. Diagrams with 3 phDP's [(a), (a'), (b), and (b')] which do not cancel in contrast with the Coulomb case, and diagrams of the same order, although with 4 phDP's [(c) and (d)], which do not cancel either. These last two diagrams correspond, in the absence of disorder, to those of Figs. 6(f)—6(i).

One can check that $[1-\overline{I}/2-(1-\overline{I})^{1/2}]$ vanishes with $\overline{I}$, like $\overline{I}^2$, and, on the other hand, does not diverge when $\overline{I}\to 1$, in contrast with (21). If I compare (29) with formula (1), $(1-\overline{I})^2\delta\chi_{\text{IF}}$, as announced in the introduction, I find a slightly different dependence in $\overline{I}$ [in particular (29) vanishes quadratically as $\overline{I}\to 0$ and not linearly like in (1)], but the same kind of overall temperature dependence is found, in particular, no divergence close to the magnetic instability, when $\overline{I}\to 1$. I discuss all the results in the following section.

IV. DISCUSSION OF THE RESULTS

(a) I chose to compute the transverse susceptibility while Ref. 2 computed the longitudinal one, but the result ought to be the same: the diagrams involved in Ref. 2 cor-

respond to those of Figs. 4 and 5, approximately dressed with phDP's. Reference 2 states that its result for the susceptibility involves diagrams shown in Figs. 7(a), 7(b), and 8(a) of Ref. 2. Such diagrams correspond, respectively, to Figs. 4(e) and 4(f) [with Green's functions dressed by impurity scattering and 3 phDP's appearing as in Figs. 12(a) and 12(a')] and to Fig. 4(c) [with 4 phDP's as schematized in Fig. 12(c)]. However, it seems that Figs. 7(c) and 7(d) in Ref. 2, although considered in the conductivity, were not considered in the susceptibility there, while they were in Ref. 11; they would correspond to my Fig. 5(d) dressed with 3 phDP's in two possible ways. But one should also consider Figs. 5(c) and 5(d) with 4 phDP's each [in that case Fig. 5(d) must be drawn as in Fig. 13]. I checked that, dressed with 4 phDP's, Figs. 4(a) and 4(b) cancel altogether—Figs. 5(a) and 5(b) as well—and also, in $(\zeta^{++}-\zeta^{+-})$, Diagrams [4(c)-5(c)-5(d)]= Diagrams [6(f) + 6(g) + 6(h) + 6(i)]. I also checked that, dressed with 3 phDP's, $2\times$ Diagram [4(d)]$-2\times$Diagram [5(d)]= $2\times$ Diagram [6(e)]. What remains with 3 phDP's are Diagrams 4(e) + 4(f) + 4(g) + 4(h), which are the same as Diagrams 6(a) + 6(b) + 6(c) + 6(d). Thus it is clear that it is simpler to deal with $\mathcal{X}^{+-}$ rather than with $\mathcal{X}^{zz}$. I suppose that the neglect of Figs. 5(c) and 5(d) with 4 phDP's and $2\times$Diagram[4(d)] and $2\times$ Diagram [5(d)] with 3 phDP's in Ref. 2 (in the Hubbard-model case) may be the source of the slight difference in the $\bar{I}$ dependence between formula (29) of the present paper and formula (1) extracted from Ref. 2.

(b) The most important point, however, is the noncancellation between the diagrams with 2 phDP's, as emphasized in the text. Comparing (21) with (29), they give contributions of the same second order in $(\epsilon_F\tau)^{-1}$. They both contribute to a decreasing temperature variation when T increases. However, (21) and (23) will predominate depending on the range of T, inside the region of interest of (12), $T\tau \ll 1$.

(i) If $T\tau < (1-\bar{I})^{1/2} \ll 1$, (29) will predominate and one will recover the overall susceptibility change proportional to $(1-\bar{I})^{-2}\sqrt{T}$, announced in Ref. 1:

$$\mathcal{X}(T)=\frac{N_0+\delta\mathcal{X}}{1-I[N_0+\delta\mathcal{X}]} \sim \frac{N_0+\delta\mathcal{X}}{(1-\bar{I})\left[1-I\dfrac{\delta\mathcal{X}}{1-\bar{I}}\right]}$$

$$\sim \frac{N_0}{1-\bar{I}}\left[1+\frac{\delta\mathcal{X}}{N_0(1-\bar{I})}\right], \quad (30a)$$

$$=\mathcal{X}(T=0)+\Delta\mathcal{X}(T), \quad (30b)$$

$$\Delta\mathcal{X}(T)\sim\frac{(\delta\mathcal{X})_{(29)}}{(1-\bar{I})^2} \propto -\frac{1}{(\epsilon_F\tau)^2}\frac{(T\tau)^{1/2}}{(1-\bar{I})^2}, \quad T\tau<(1-\bar{I})^{1/2}$$

$$(31)$$

where $(\delta\mathcal{X})_{(29)}$ is the T dependence of the contribution of formula (29) $[(\delta\mathcal{X})_{3\text{ phDP's}}+(\delta\mathcal{X})_{4\text{ phDP's}}]$. Note that (31) yields an infinite slope when $T\to 0$.

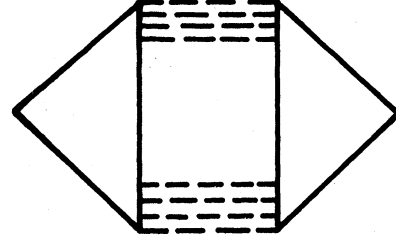(ii) However, when $(1-\bar{I})^{1/2} < T\tau \ll 1$, a range which

FIG. 13. Another way of drawing Fig. 5(d), which is identical to it in the absence of disorder, but which may be dressed with 4 phDP's, while Fig. 5(d), as such, must be dressed with 3 phDP's in two possible ways as in Figs. 7(c) and 7(d) of Ref. 2, or the two possible ways in Fig. 1(b) of Ref. 11.

may be reached at quite a low temperature if the pure system is strongly enhanced ($\bar{I}$ is close to 1), then (21) will predominate over (29) and one gets, analogously to (30) and (31),

$$\Delta\mathcal{X}(T)\sim\frac{(\delta\mathcal{X})_{(21)}}{(1-\bar{I})^2} \propto -\frac{1}{(\epsilon_F\tau)^2}\frac{(T\tau)^{3/2}}{(1-\bar{I})^2(1-\bar{I})^{1/2}},$$

$$(1-\bar{I})^{1/2}<T\tau\ll 1 \quad (32)$$

where $(\delta\mathcal{X})_{(21)}$ is the T dependence of the contribution of formula (21): $(\delta\mathcal{X})_{2\text{ phDP's}}$.

(iii) What is more important is the contribution of disorder to $\mathcal{X}(T=0)$. At $T=0$, (21) clearly predominates with the large contribution $(1-\bar{I})^{-1/2}$. Therefore, in the first expression in (30a), one has

$$1-I[N_0+(\delta\mathcal{X})_{T=0}]=1-I\left[N_0+\frac{\sqrt{3}N_0}{(\epsilon_F\tau)^2}\frac{1}{(1-\bar{I})^{1/2}}\right]$$

$$=1-\bar{I}\left[1+\frac{\sqrt{3}}{(\epsilon_F\tau)^2}\frac{1}{(1-\bar{I})^{1/2}}\right].$$

$$(33)$$

Therefore, even though we are in the weak localization regime,

$$\epsilon_F\tau \gg 1 \quad (34)$$

since, near the magnetic instability,

$$(1-\bar{I})^{-1} \gg 1, \quad (35)$$

the contribution $[\sqrt{3}(\epsilon_F\tau)^{-2}(1-\bar{I})^{-1/2}]$ in (33) may be non-negligible compared to unity. Such a correction yields an effective value $\bar{I}_{\text{eff}}$ for $\bar{I}$:

$$\bar{I}_{\text{eff}}=\bar{I}\left[1+\frac{\sqrt{3}}{(\epsilon_F\tau)^2}\frac{1}{(1-\bar{I})^{1/2}}+\cdots\right]. \quad (36)$$

At that order in $(\epsilon_F\tau)^{-1}$, $\bar{I}_{\text{eff}}$ is larger than $\bar{I}$. Such a result is in agreement with what was conjectured in Ref. 4: that paramagnons (stronger in the presence of disorder[4]) contribute to yield a larger Stoner enhancement than in the absence of disorder; indeed I find

$$\frac{\chi(T=0)}{N_0} = \frac{1}{1-\bar{I}_{\text{eff}}}$$

$$= \frac{1}{1-\bar{I}} \left[1 + \frac{\sqrt{3}}{(\epsilon_F \tau)^2} \frac{\bar{I}}{(1-\bar{I})^{3/2}} \right] > \frac{1}{1-\bar{I}} . \quad (37)$$

This also goes along with the general tendency found in Ref. 5. However, the theory here is a perturbative one, which means that one is confined to

$$\frac{1}{(\epsilon_F \tau)^2} < (1-\bar{I})^{3/2} . \quad (38)$$

In other words, one is not only in the weakly localized regime, but also not too close to the magnetic instability. Were we much closer to it, for $\bar{I}$ very close to 1, (38) could no longer hold and the expansion (36) would break down.

(c) Finally, it is hopefully clear that more sophisticated theories like the one of Ref. 5 dealing with the screened Coulomb interaction do not cover the contact interaction since they ought to not only let the range of the interaction become very small, but at the same time impose spin constraints, which will at once make the three different structures $\tilde{\chi}_l$, $\tilde{\chi}_{ro}$, and $\tilde{\chi}_{re}$ appear (instead of the unique one V_s), which in turn are the source of the extra contribution obtained here.

(d) I have confined consideration in this paper to phDP's in order to dress the various diagrams contributing to the susceptibility in the presence of weak disorder and a strong interaction. It remains to include the contribution of ppDP's as well, and to look for both their effects on other properties: specific heat, conductivity, etc.

(e) One last remark concerns the conjecture, proposed in Ref. 4(b) that paramagnons altogether become stronger and tend to become local in the presence of disorder, in which case one might have a crossover towards a regime of vanishing interaction, enabling the metal-insulator transition to take place. This will occur if, for increasing disorder, the space dependence of the paramagnons disappears *before* the magnetic instability is reached. One should then (again for stronger disorder than in the present paper) study, on equal footing, the effect of disorder on the paramagnon space dependence as well as on the effective value of the Stoner enhancement. This appears, at present, difficult.

APPENDIX A: COMPARISON BETWEEN THE CONDUCTIVITY DIAGRAMS CONTAINING THE phDP'S IN THE CASE OF THE SCREENED COULOMB INTERACTION AND IN THE PARAMAGNON CASE

In Appendix A, I follow step by step, the Appendix C of Ref. 10, to demonstrate that, in comparison with the Coulomb interaction case of Ref. 10, instead, for the Hubbard-type contact interaction treated here, the corresponding diagrams *do not cancel*. As in Ref. 10, I separate the integral over momentum of the product of the ^{2}phDP's by the interaction [$V_s(q,\omega)$ in Ref. 10 and $\tilde{\chi}(q,\omega)$ in the present paper]:

$$f(\omega) = \int \frac{d^3 q}{(2\pi)^3} \frac{\tilde{\chi}(q,\omega)}{\tau^2 (Dq^2 - i\omega)^2} . \quad (A1)$$

The space dimensionality, as will be clear later, plays no role in the cancellation or combination of the diagrams.

Compared to V_s which assumed a unique form, we will have here three possibilities for the paramagnon structure of the type of Fig. 1 but renormalized by impurity scattering, as explained in the text in formulas (18), $\tilde{\chi}_{ro}$, $\tilde{\chi}_{re}$, and $\tilde{\chi}_l$. The corresponding integrals in (A1) will be called f_{ro}, f_{re}, and f_l. I then compute the diagrams of Figs. 11(a)—11(c), analogous to those of Figs. 5(a)—5(c) of Ref. 10. I will use here the same notation that appears in Appendix C of Ref. 10 (a_{++}, etc.) with the exact limits of integration [note that, instead, in formula (C2) of Ref. 10, the integral over ϵ has been approximated by $\int_0^\infty d\epsilon$ although, as is obvious from the limits over ω, it should rather read $\int_0^{1/\tau - \Omega} d\epsilon$]. I will have two types of diagrams in Figs. 11(a) and 11(c), one with $\tilde{\chi}_l$, the other with $\tilde{\chi}_{ro}$, which will be contained in $(f_l + f_{ro})$. I then get

$$a_{++} = \int_0^{1/\tau - \Omega} d\epsilon \int_{-1/\tau}^{-(\epsilon + \Omega)} d\omega [f_{ro}(-\omega) + f_l(-\omega)] \sum_{\mathbf{p}} p_F^2 G_+^3(\mathbf{p}) G_-(\mathbf{p}) = a'_{++} , \quad (A2)$$

$$a_{--} = \int_{-1/\tau - \Omega}^{-\Omega} d\epsilon \int_{-(\epsilon + \Omega)}^{1/\tau} d\omega [f_{ro}(\omega) + f_l(\omega)] \sum_{\mathbf{p}} p_F^2 G_-^3(\mathbf{p}) G_+(\mathbf{p}) = a'_{--} , \quad (A3)$$

$$a_{-+} = \int_{-\Omega}^0 d\epsilon \int_{-1/\tau}^{-(\epsilon + \Omega)} d\omega [f_{ro}(-\omega) + f_l(-\omega)] \sum_{\mathbf{p}} p_F^2 G_+^2(\mathbf{p}) G_-^2(\mathbf{p}) = a'_{-+} , \quad (A4)$$

$$b_{++} = \int_0^{1/\tau - \Omega} d\epsilon \int_{-1/\tau}^{-(\epsilon + \Omega)} d\omega f_{re}(-\omega) \sum_{\mathbf{p}} p_F^2 G_+^2(\mathbf{p}) G_-^2(\mathbf{p}) , \quad (A5)$$

$$b_{--} = \int_{-1/\tau}^{-\Omega} d\epsilon \int_{-\epsilon}^{1/\tau} d\omega f_{re}(\omega) \sum_{\mathbf{p}} p_F^2 G_+^2(\mathbf{p}) G_-^2(\mathbf{p}) , \quad (A6)$$

$$c_{-+} = \int_{-\Omega}^{0} d\epsilon \int_{-1/\tau}^{-(\epsilon+\Omega)} d\omega [f_{ro}(-\omega)+f_I(-\omega)] \sum_{p} p_F^2 G_+^2(\mathbf{p})G_-(\mathbf{p}) \sum_{p'} G_+^2(\mathbf{p}')G_-(\mathbf{p}') = c'_{-+} \tag{A7}$$

with

$$U^2 = \frac{1}{2\pi N_0 \tau} . \tag{A8}$$

It is easy to verify that (as done in Appendix B of the present paper), as in the two-dimensional (2D) case of Ref. 10, one has in 3D as well,

$$P = \sum_{p} p_F^2 G_+^3 G_- = \sum_{p} p_F^2 G_+ G_-^3$$

$$= -\tfrac{1}{2} \sum_{p} p_F^2 G_+^2 G_-^2 = -2\pi p_F^2 N_0 \tau^3 , \tag{A9}$$

$$U^2 p_F^2 \sum_{p} G_+^2 G_- \sum_{p'} G_+^2 G_- = p_F^2 (-2i\pi N_0 \tau^2)^2 \frac{1}{2\pi N_0 \tau}$$

$$= -2\pi p_F^2 N_0 \tau^3 = P . \tag{A10}$$

Changing the variables in (A2)–(A7), so that variables of integration will be positive, and setting $\epsilon = \Omega + \epsilon'$ in a_{--}, a'_{--}, and b_{--} and $\epsilon + \Omega = \epsilon''$ in b_{++}, one finally gets

$$a_{++} + a'_{++} = 2P \int_0^{1/\tau - \Omega} d\epsilon \int_{\epsilon + \Omega}^{1/\tau} d\omega [f_{ro}(\omega) + f_I(\omega)] , \tag{A11}$$

$$a_{--} + a'_{--} = 2P \int_0^{1/\tau} d\epsilon \int_{\epsilon}^{1/\tau} d\omega [f_{ro}(\omega) + f_I(\omega)] , \tag{A12}$$

$$a_{-+} + a'_{-+} = -4P \int_0^{\Omega} d\epsilon \int_{\Omega-\epsilon}^{1/\tau} d\omega [f_{ro}(\omega) + f_I(\omega)] , \tag{A13}$$

$$c_{-+} + c'_{-+} = 2P \int_0^{\Omega} d\epsilon \int_{\Omega-\epsilon}^{1/\tau} d\omega [f_{ro}(\omega) + f_I(\omega)] , \tag{A14}$$

$$b_{++} = -2P \int_{\Omega}^{1/\tau} d\epsilon \int_{\epsilon}^{1/\tau} d\omega f_{re}(\omega) , \tag{A15}$$

$$b_{--} = -2P \int_0^{1/\tau - \Omega} d\epsilon \int_{\Omega+\epsilon}^{1/\tau} d\omega f_{re}(\omega) . \tag{A16}$$

Then one has

$$a_{++} + a'_{++} + b_{--}$$
$$= 2P \int_0^{1/\tau - \Omega} d\epsilon \int_{\Omega+\epsilon}^{1/\tau} d\omega [(f_{ro}+f_I) - f_{re}] , \tag{A17}$$

$$a_{-+} + a'_{-+} + c_{-+} + c'_{-+}$$
$$= -2P \int_0^{\Omega} d\epsilon \int_{\Omega-\epsilon}^{1/\tau} [f_{ro}+f_I] . \tag{A18}$$

Separating in

$$(a_{--} + a'_{--}), \quad \int_0^{1/\tau} d\epsilon = \int_0^{\Omega} d\epsilon + \int_{\Omega}^{1/\tau} d\epsilon ,$$

one has

$$a_{--} + a'_{--} + b_{++}$$
$$= 2P \int_0^{\Omega} d\epsilon \int_{\epsilon}^{1/\tau} d\omega [f_{ro}+f_I]$$
$$+ 2P \int_{\Omega}^{1/\tau} d\epsilon \int_{\epsilon}^{1/\tau} d\omega [(f_{ro}+f_I) - f_{re}] . \tag{A19}$$

In the second term of (A19), one sets $\epsilon = \Omega + \epsilon'$ to appear similar to a term like (A17); then

$$a_{--} + a'_{--} + b_{++}$$
$$= 2P \int_0^{\Omega} d\epsilon \int_{\epsilon}^{1/\tau} d\omega [f_{ro}+f_I]$$
$$+ 2P \int_0^{1/\tau - \Omega} d\epsilon \int_{\Omega+\epsilon}^{1/\tau} d\omega [(f_{ro}+f_I) - f_{re}] . \tag{A20}$$

Then the first term of (A20) combines with (A18):

$$\int_0^{\Omega} d\epsilon \int_{\epsilon}^{1/\tau} d\omega - \int_0^{\Omega} d\epsilon \int_{\Omega-\epsilon}^{1/\tau} d\omega$$
$$= \int_0^{\Omega} d\epsilon \int_{\epsilon}^{\Omega-\epsilon} d\omega$$
$$= \int_0^{\Omega} d\epsilon \int_0^{\Omega-\epsilon} d\omega - \int_0^{\Omega} d\epsilon \int_0^{\epsilon} d\omega . \tag{A21}$$

In the first term of the last expression, one sets $\epsilon' = \Omega - \epsilon$ so that one gets

$$\int_0^{\Omega} d\epsilon \int_0^{\Omega-\epsilon} d\omega = -\int_{\Omega}^0 d\epsilon \int_0^{\epsilon} d\omega = \int_0^{\Omega} d\epsilon \int_0^{\epsilon} d\omega , \tag{A22}$$

which exactly cancels the second term in the last expression of (A21). Therefore one is finally left with only (A17) and the second term in the right-hand side of (A20):

$$a_{++} + a'_{++} + b_{--} + a_{-+} + a'_{-+} + c_{-+} + c'_{-+} + a_{--} + a'_{--} + b_{++} = 4P \int_0^{1/\tau - \Omega} d\epsilon \int_{\Omega+\epsilon}^{1/\tau} d\omega [(f_{ro}+f_I) - f_{re}] . \tag{A23}$$

It is clear that, if the sum $(f_{ro}+f_I)$ as well as f_{re} would reduce to $V_s(q,\omega)$ as in Ref. 10, the quantity in the square brackets of (A23) would identically vanish and one would recover the cancellation proved in Appendix C of Ref. 10. Instead here we have

$$[(f_{ro}+f_I) - f_{re}] = \int \frac{d^3\mathbf{q}}{(2\pi)^3} \frac{1}{\tau^2(Dq^2 - i\omega)^2}$$
$$\times [(-\widetilde{\chi}_{ro}) + (\widetilde{\chi}_I) - (-\widetilde{\chi}_{re})] . \tag{A24}$$

The signs in (A24) must be understood as follows, with the conventions at the end of Sec. II: in the diagrams involving $\widetilde{\chi}_{ro}$ or $\widetilde{\chi}_{re}$ one has, aside from these paramagnon propagators [evaluated in formula (18) of the text], one extra big loop and therefore one extra minus sign in both cases; in the diagrams involving $\widetilde{\chi}_I$, one has two extra big loops and thus a plus sign. In (A24) the combination of the $\widetilde{\chi}$'s reads

$$(\widetilde{\chi}_l) + (-\widetilde{\chi}_{ro}) - (-\widetilde{\chi}_{re}) = \left[-\frac{I^2\widetilde{\chi}_0}{1-I\widetilde{\chi}_0} \right] + \left[-\frac{I^2\widetilde{\chi}_0}{1-I^2\widetilde{\chi}_0^2} \right] - \left[+\frac{I^3\widetilde{\chi}_0^2}{1-I^2\widetilde{\chi}_0^2} \right]$$

$$= -\frac{I^2\widetilde{\chi}_0}{1-I\widetilde{\chi}_0} - \frac{I^2\widetilde{\chi}_0(1+I\widetilde{\chi}_0)}{(1-I\widetilde{\chi}_0)(1+I\widetilde{\chi}_0)} = -\frac{2I^2\widetilde{\chi}_0}{1-I\widetilde{\chi}_0} ,$$

$$\text{(A25)}$$

with

$$\widetilde{\chi}_0(q,\omega) = N_0 \frac{Dq^2}{Dq^2 - i\omega} . \qquad \text{(A26)}$$

$\widetilde{\chi}_{ro}$ and $\widetilde{\chi}_{re}$ having one minus sign difference, combine to yield a contribution of the same form as $\widetilde{\chi}_l$. This is linked to their having one bubble difference, itself due to the bare interaction I playing a role only among opposite spins.

Therefore the same diagrams with 2 phDP's, considered in Ref. 10 and here, yield different conclusions: they cancel in the case of the screened Coulomb interaction while they combine to give a finite contribution in the paramagnon case. [Note in passing that the diagrams of Fig. 11(c) contribute a vanishing contribution, as they should, when $\Omega \to 0$.] The usual scaling argument tells us at once that these diagrams with 2 phDP's, when they do not cancel, give a temperature dependence proportional to $T^{3/2}$ in three dimensions. As far as the two-dimensional paramagnon case is concerned, it exhibits severe specific difficulties, both in the pure and in the disordered cases,[12] so I do not wish to elaborate more on it here. In any case, it is clear that the screened Coulomb interaction considered in Ref. 10 cannot, as it stands, recover the contact interaction case without not only reducing the screening

length, but most importantly, examining in detail the *restrictions* implied in the diagrams by *spin constraints*.

APPENDIX B: CALCULATION OF A NUMBER OF USEFUL INTEGRALS

I compute first

$$\int G^3 G = \int \frac{d^3p}{(2\pi)^3} G^3(\mathbf{p},\widetilde{\omega}_n) G(\mathbf{p}+\mathbf{q},\widetilde{\omega}_{n+\nu})$$

$$\simeq N_0 \int_{-1}^{+1} \frac{dz}{2} \int \frac{d\xi}{(\xi - i\widetilde{\omega}_n)^3(\xi + p_F qz - i\widetilde{\omega}_{n+\nu})} ,$$

$$\text{(B1)}$$

where $\xi_{\mathbf{p}+\mathbf{q}}$ is approximated, as usual, for small q values by

$$\xi_{\mathbf{p}+\mathbf{q}} \simeq \xi_p + p_F qz = \xi + p_F qz ,$$

$$z = \cos(\mathbf{p},\mathbf{q}) = \cos\theta . \qquad \text{(B2)}$$

As usual, to have the diffusion pole appearing in the diagrams computed in the text, one is always restricted to

$$\omega_n, \omega_{n+\nu} < 0 . \qquad \text{(B3)}$$

Then

$$\int G^3 G = N_0 \int_{-1}^{+1} \frac{dz}{2} 2i\pi \left[\frac{\Theta(\omega_{n+\nu})\Theta(-\omega_n)\Theta(\omega_\nu)}{(i\omega_\nu + i/\tau - p_F qz)^3} - \frac{\Theta(\omega_n)\Theta(-\omega_{n+\nu})\Theta(-\omega_\nu)}{(i\omega_\nu - i/\tau - p_F qz)^3} \right] \qquad \text{(B4)}$$

$$\simeq -2\pi N_0 \tau^3 [\Theta(\omega_{n+\nu})\Theta(-\omega_n)\Theta(\omega_\nu) + \Theta(\omega_n)Q(-\omega_{n+\nu})\Theta(-\omega_\nu)] , \qquad \text{(B5)}$$

where I have used the fact that $|\omega_\nu|\tau \ll 1$ and $p_F q\tau \ll 1$. Note that

$$T\sum_n \int G^3 G = -N_0 \tau^3 |\omega_\nu| . \qquad \text{(B6)}$$

On the other hand

$$\int G^2 G^2 = \int \frac{d^3p}{(2\pi)^3} G^2(\mathbf{p},\omega_n) G^2(\mathbf{p}+\mathbf{q},\omega_{n+\nu}) \simeq N_0 \int_{-1}^{+1} \frac{dz}{2} \frac{d\xi}{(\xi - i\widetilde{\omega}_n)^2(\xi + p_F qz - i\widetilde{\omega}_{n+\nu})} \qquad \text{(B7)}$$

$$\simeq 4\pi N_0 \tau^3 [\Theta(\omega_{n+\nu})\Theta(-\omega_n)\Theta(\omega_\nu) + \Theta(\omega_n)\Theta(-\omega_{n+\nu})\Theta(-\omega_\nu)] . \qquad \text{(B8)}$$

Note that

$$T\sum_n \int G^2 G^2 = +2N_0 \tau^3 |\omega_\nu| . \qquad \text{(B9)}$$

I will also need

$$\int G^2 G = \int \frac{d^3\mathbf{p}}{(2\pi)^3} G^2(\mathbf{p},\widetilde{\omega}_n) G(\mathbf{p}+\mathbf{q},\widetilde{\omega}_{n+\nu}) \simeq -N_0 \int_{-1}^{+1} \frac{dz}{2} \int \frac{d\xi}{(\xi - i\widetilde{\omega}_n)^2 (\xi + p_F q z - i\widetilde{\omega}_{n+\nu})} \, , \tag{B10}$$

$$\simeq 2i\pi N_0 \tau^2 [\Theta(\omega_{n+\nu})\Theta(-\omega_n)\Theta(\omega_\nu) - \Theta(\omega_n)\Theta(-\omega_{n+\nu})\Theta(-\omega_\nu)] \, , \tag{B11}$$

and

$$-T\sum_n \int \frac{d^3p}{(2\pi)^3} G^2(\mathbf{p},\widetilde{\omega}_n) G(\mathbf{p}+\mathbf{q},\widetilde{\omega}_{n+\nu}) = -iN_0 \tau^2 \omega_\nu \, . \tag{B12}$$

One also checks that

$$\int G^2(\mathbf{p},\widetilde{\omega}_n) G(\mathbf{p}-\mathbf{q},\widetilde{\omega}_{n-\nu}) \frac{d^3\mathbf{p}}{(2\pi)^3} \simeq 2i\pi N_0 \tau^2 [\Theta(\omega_{n-\nu})\Theta(-\omega_n)\Theta(-\omega_\nu) - \Theta(\omega_n)\Theta(-\omega_{n-\nu})\Theta(\omega_\nu)] \, , \tag{B13}$$

$$\int G^2(\mathbf{p}+\mathbf{q},\widetilde{\omega}_{n+\nu}) G(\mathbf{p},\widetilde{\omega}_n) \frac{d^3\mathbf{p}}{(2\pi)^3} \simeq 2i\pi N_0 \tau^2 [\Theta(\omega_n)\Theta(-\omega_{n+\nu})\Theta(-\omega_\nu) - \Theta(\omega_{n+\nu})\Theta(-\omega_n)\Theta(\omega_\nu)] \, , \tag{B14}$$

and

$$-T\sum_n \int G^2(\mathbf{p},\widetilde{\omega}_n) G(\mathbf{p}-\mathbf{q},\widetilde{\omega}_{n-\nu}) = -T\sum_n \int \frac{d^3p}{(2\pi)^3} G^2(\mathbf{p}+\mathbf{q},\widetilde{\omega}_{n+\nu}) G(\mathbf{p},\widetilde{\omega}_n) = iN_0 \tau^2 \omega_\nu \, . \tag{B15}$$

[1]B. L. Al'tshuler and A. G. Aronov, Zh. Eksp. Teor. Fiz. **77**, 2028 (1979) [JETP **50**, 969 (1979)], note just before formula (3) of that paper a slight misprint: $\gamma \ll 1$ is not the Stoner enhancement but its inverse.

[2]Y. Isawa and H. Fukuyama, J. Phys. Soc. Jpn. **53**, 1415 (1984).

[3](a) M. T. Béal-Monod, S.-k. Ma, and D. R. Fredkin, Phys. Rev. Lett. **20**, 929 (1968); (b) S.-k. Ma, M. T. Béal-Monod, and D. R. Fredkin, Phys. Rev. **174**, 227 (1968).

[4](a) M. T. Béal-Monod, Phys. Rev. B **31**, 1647 (1985); (b) **32**, xxxx (1985).

[5]A. M. Finkel'stein, Z. Phys. B **56**, 189 (1984); Pis'ma Zh. Eksp. Teor. Fiz. **84**, 168 (1983) [JETP Lett. **40**, 796 (1984)]; **40**, 63 (1984); **40**, 796 (1984)]; C. Castellani et al., Phys. Rev. B **30**, 527 (1984); **30**, 1593 (1984); **30**, 1596 (1984).

[6]A. Layzer and D. Fay Int. J. Magn. **1**, 135 (1971); N. F. Berk and J. R. Schrieffer, Phys. Rev. Lett. **17**, 433 (1966).

[7]M. T. Béal-Monod, K. Maki, and J. P. Hurault, J. Low Temp. Phys. **17**, 439 (1974); in formula (2) of that paper, the coefficient in front of the right-hand side should read $\frac{1}{2}$ instead of $\frac{1}{4}$.

[8]A. A. Abrikosov, L. P. Gor'kov, and I. Dzyaloshinski, Methods of Quantum Field Theory in Statistical Physics (Prentice-Hall, Englewood Cliffs, N.J., 1963).

[9]H. Fukuyama, J. Phys. Soc. Jpn. **50**, 3407 (1981).

[10]B. L. Al'tshuler, D. Khmel'nitzkii, A. I. Larkin, and P. A. Lee, Phys. Rev. B **22**, 5142 (1980).

[11]B. L. Al'tshuler, A. G. Aronov, and A. Yu. Zyuzin, Pis'ma Zh, Eksp. Teor. Fiz. **35**, 15 (1982) [JETP Lett. **35**, 16 (1982)].

[12]A. Theumann and M. T. Béal-Monod, Phys. Rev. B **29**, 2567 (1984); M. T. Béal-Monod, ibid. **31**, 2764 (1985).